https://dx.doi.org/10.1016/j.buildenv.2021.108224

Spatiotemporal impact of vehicle heat on urban thermal environment: a case study of Hong Kong

Xuan Chen[1], Jiachuan Yang[1,*], Rui Zhu[2], Man Sing Wong[2], Chao Ren[3]

[1]Department of Civil and Environmental Engineering, The Hong Kong University of Science and Technology, Hong Kong, China

[2]Department of Land Surveying and Geo-Informatics, The Hong Kong Polytechnic University, Hong Kong, China

[3]Faculty of Architecture, The University of Hong Kong, Hong Kong, China

*Correspondence to: cejcyang@ust.hk; Tel: +852-2358-8184; Fax: +852-2358-1534;

Abstract

Vehicle heat (VH) is a substantial portion of anthropogenic heat emission and modifies the urban thermal environment. Quantifying the impact of VH has implications for the potential benefits of electric vehicles in cities, yet the spatiotemporal impact of VH has not been investigated separately. In this study, we incorporate VH and urban landscape data into the Weather Research and Forecasting (WRF) model to estimate the VH impacts at a fine spatial resolution over Hong Kong. Results show a strong temporal variation of the VH impact at both weekly and seasonal scales: 1) increases in sensible heat is more pronounced during weekdays than weekends, 2) the warmth of urban canyon air temperature is 0.35 °C in winter and 0.21 °C in summer over the VH emission area. In terms of the spatial variation, increased air temperature over land by VH is found to have a positive relationship with urban area fraction and building height, but not the aspect ratio. The statistically significant VH impact (90% confidence level) has the largest spatial coverage during 8 pm – 10 pm local time in Hong Kong. The significant VH impact exists in low urbanized areas with highways and circulation roads, and in densely built-up areas with high urban area fraction or/and high-rise buildings, especially in daytime rush hours and on winter nights. The temporal differences and spatial distributions of the VH impact provide insights into the environmental benefits of green transportation policy.

Keywords:

Vehicle heat, Urban thermal environment, Urban morphology, WRF simulation

1. Introduction

Anthropogenic heat (AH) and land cover modification are two main contributors to the higher temperature in cities, a phenomenon called the urban heat island (UHI). Although cities only cover less than 5% of the earth surface, they accommodate 55% of the world's population and are responsible for 70% of the world's energy demand (Gago et al., 2013, Madlener & Sunak, 2011; United Nations, 2018). Concentrated release of AH in this small percentage of the earth surface thus has large adverse impacts on global human health and energy sustainability (Salvati et al., 2017; Santamouris et al., 2001; Sun et al., 2018). Building heat emission, vehicle waste heat and metabolic heat from people are the three main components of AH. The release of AH is spatially varied over different urban land uses, generally being more significant in industry and commercial areas, or/and along the highways/free-ways (Allen et al., 2011; Chen et al., 2016). The temporal variation of AH is also evident (Sun et al., 2018): daily peak fluxes coincide with morning and evening rush hour periods, and the cold season tends to have a larger emission than the warm season in mid/high latitude cities. To estimate the amount of AH releases in a city, one of the most reliable methods is based on an inventory approach. This method estimates each component of the AH separately and has been applied to cities around the world (Sailor, 2011; Sailor and Lu, 2004; Smith et al., 2009;). Increased data availability in recent years allows the estimation of AH emissions at fine spatiotemporal resolutions. For example, Iamarino et al. (2012) estimated the AH emissions for London at a resolution of 30 mins and 200 × 200 m^2, Chow et al. (2014) produced hourly AH data with a 1 × 1 km^2 resolution for Phoenix, and Molnár et al. (2020) estimated the peak values of AH profiles for different Local Climate Zones (Stewart and Oke., 2012).

As an additional energy source in the urban environment, AH can modify the intensity and variability of urban heat island (Bohnenstengel et al., 2014), aggravate/alleviate the thermal discomfort under heat/cold waves (Li & Bou-Zeid, 2013; Yang & Bou-Zeid, 2018), and affect the structure of the atmospheric boundary layer and urban rainfall pattern (Nie et al., 2017). Thus, quantifying the impact of AH on the urban climate has become a topic as essential as estimating the emission amount. The topic has been investigated through numerical weather simulations in the literature. Block et al. (2004) found that a 20 W m^{-2} AH could rise the air temperature by 0.5 °C in the populated Ruhr region of Germany, Fan & Sailor (2005) reported that the AH release in winter could rise the nighttime air temperature by 2 – 3 °C in Philadelphia, and Yang et al. (2019) suggested that the AH release increased urban air temperature by around

1°C in the Yangtze River Delta region. The AH-induced modification of urban climate has substantial seasonal variation. Chen et al. (2016) found the AH contributed 65% of the UHI intensity in winter and 17% in summer over the Chinese city Hangzhou.

As the most significant portion of AH in general, the impact of building heat emission has drawn many attentions. For example, Salamanca et al. (2014) quantified the impact of the heat released from the air conditioning systems over the Phoenix metropolitan area, US, and later Wang et al. (2018) quantified this aspect for Hong Kong. However, vehicle heat (VH), which is generally recognized as the second-largest portion of the AH (Quah & Roth., 2012; Smith et al., 2009), has been rarely investigated regarding its separate impact on urban climate. For instance, VH contributes 47% of the AH in São Paulo, Brazil (Ferreira et al., 2011), and is the major source of AH during summer in France (Pigeon et al., 2007). Compared to building heat emission, VH is released in the traffic flow associated with residents' commuting pattern, and consequently the spatiotemporal distribution of VH release has great influences on residents' exposure to thermal discomfort (Yang et al., 2019). Zhu et al. (2017) estimated hourly gridded VH profiles in Hong Kong and found a robust correlation between VH and UHI intensity. They suggested the VH could be a critical driver for UHI at locations surrounded by high-rise buildings, with dense vehicle flows, and at seaside where VH is the single contributor for AH. Until now, the spatial and temporal variations of the impact of VH on the thermal environment over diverse urban landscapes remain unclear.

For mitigation and adaptation to global warming, governments have encouraged high energy-efficient electric vehicles as a measure to reduce greenhouse gas emissions in the past decade (World Energy Outlook, 2019). Quantifying the spatiotemporal impact of VH on the urban thermal environment is therefore imperative as it could provide insights into the potential benefit of electric vehicles. It is worth noting that Singh et al. (2020) estimated the impact of VH over Singapore by integrating hourly spatial VH data into regional climate simulations during April 2016. They found that VH increased the air temperature nearly 1.1 °C during the morning peak period. However, the study used a mean VH profile for the entire simulation period that the differences between weekday and weekend is neglected.

In the present study, we choose Hong Kong as an example to investigate the spatiotemporal impact of vehicle heat on urban thermal environment. Hong Kong is a dense east Asian city with a population of more than 7 million. Because of the multitude of challenges presented by

Hong Kong's natural and urban landscapes, substantial research efforts have devoted to urban climate studies on this city as a typical test case (Cai et al., 2020; Liu et al., 2020; Wang et al., 2020). Due to its high development level, Hong Kong has a daily AH emission of around 300 W m^{-2} in autumn (Wong et al., 2015), resulting in an intense UHI phenomenon (Chen & Jeong, 2018). Previous studies examining waste heat impact were limited to the low spatial resolution or short study periods. To overcome the limitation, this study aims to quantify the spatial variation of VH impact on the thermal environment over diverse urban landscape, and the temporal variation of VH impact at multiple time scales (daily, weekly and seasonal). Towards this end, the study integrated fine-resolution urban canopy data (Wong et al., 2019; Zheng et al., 2018) and vehicle heat data (Zhu et al., 2017) into numerical weather simulations over Hong Kong. The relationship between the impact of vehicle heat and urban morphological parameters is analyzed.

2. Methodology

2.1 High-resolution weather simulation

The Weather Research and Forecasting (WRF) model version 3.8.1 (Skamarock et al., 2008) coupled with a single-layer urban canopy model (SLUCM, Kusaka et al., 2001; Yang et al., 2015) was adopted for performing weather simulations in this study. Four one-way nested domains were generated with horizontal grid resolutions of 13.5 km (d01; mesh size of 180 × 180), 4.5 km (d02; mesh size of 271 × 271), 1.5 km (d03; mesh size of 301 × 301), and 500 m (d04; mesh size of 409 × 409) (Fig. 1a). The innermost domain (d04) was centered at Hong Kong and covered the entire Greater Bay Area (Fig. 1b). The vertical grid contained 35 full sigma levels from the surface up to 50 hPa. The physical parameterization schemes were chosen as follows: (1) the WSM 6-class graupel scheme for microphysics (Hong & Lim, 2006); (2) the Dudhia (Dudhia, 1989) and RRTM scheme (Mlawer et al., 1997) for shortwave and longwave radiation, respectively; (3) the Eta similarity scheme (Janjić, 1994) for the surface layer; (4) the Yonsei University planetary boundary layer scheme (Noh et al., 2003); and (5) the Noah LSM scheme (Chen and Dudhia, 2001) for the land surface process over natural land cover. The initial and boundary conditions were derived from the 6-hourly Global Final Analysis data of the National Center for Environmental Prediction at a 1° × 1° resolution (http://rda.ucar.edu/datasets/ds083.2/). The United States Geological Survey (USGS) land cover classification data with 28 categories was used in this study.

In the default WRF simulations, the land use condition of each grid is determined by the dominant land cover type. A grid is considered as an urban grid when the fraction of urban land use exceeds that of other individual land use types. The SLUCM model is called to solve heat and moisture budgets only over urban grids. To better represent the land use condition, despite the dominant land cover type, we turned on the SLUCM for all grids with an impervious surface fraction larger than zero. The urban portion is solved by the SLUCM, and the non-urban portion is set as the original land use type according to the USGS map and is modelled using the Noah LSM scheme. The meteorological variables over these grids are estimated by weighted averaging the urban and non-urban areas. The waste heat by vehicles is assumed to be released in the urban portion of each grid.

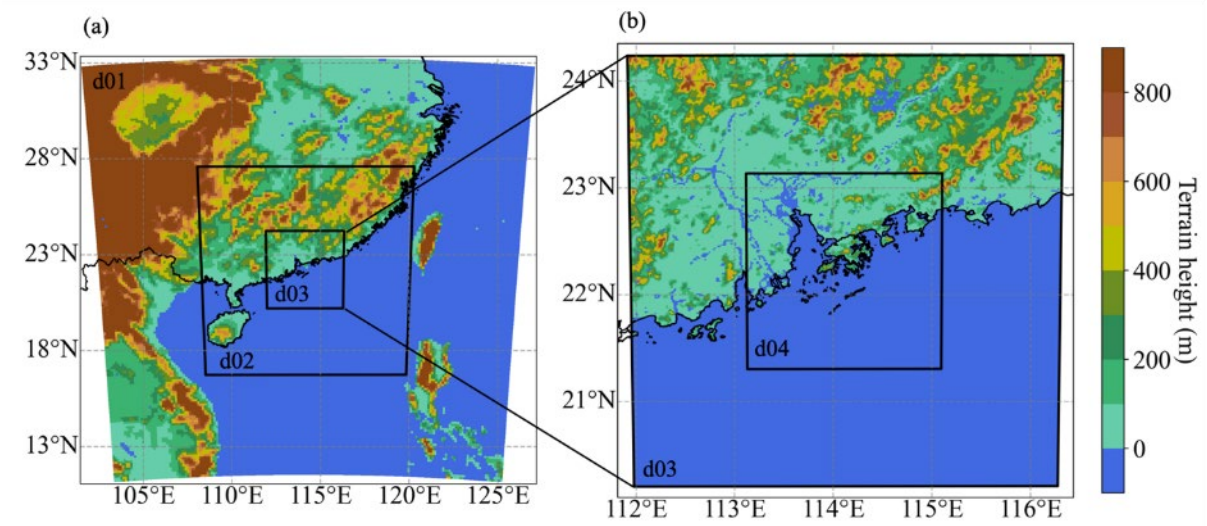

Fig. 1. Nested domain configuration for WRF simulations with a horizontal grid spacing of 13.5 km (d01), 4.5 km (d02), 1.5 km (d03), and 0.5 km (d04) overlaid with the terrain height. The study area Hong Kong is at the centre of the innermost domain (d04).

2.2 Urban canopy parameter

To better represent the heterogeneous urban landscape, we incorporated the urban canopy parameters (UCPs) into the WRF simulations based on the 2016 local climate zone (LCZ) map in this study. The LCZ map was developed using an improved method of the World Urban Database and Portal Tool (WUDAPT) and its overall accuracy reaches 76% (Ren et al., 2019). A set of urban canopy parameters, including mean building height, street width, building width, standard deviation of building height, plan area fraction and urban fraction, is specified for each urban local climate zone. The resolution of the LCZ map is 100 m × 100 m. To be consistent with the grid resolution in WRF d04 (500 m × 500 m), the values of UCPs in each

WRF d04 grid is equal to the average of the nearest 25 LCZ grids (Wong et al., 2019). Figure 2 shows the spatial distribution of the urban canopy parameters used in the WRF simulations.

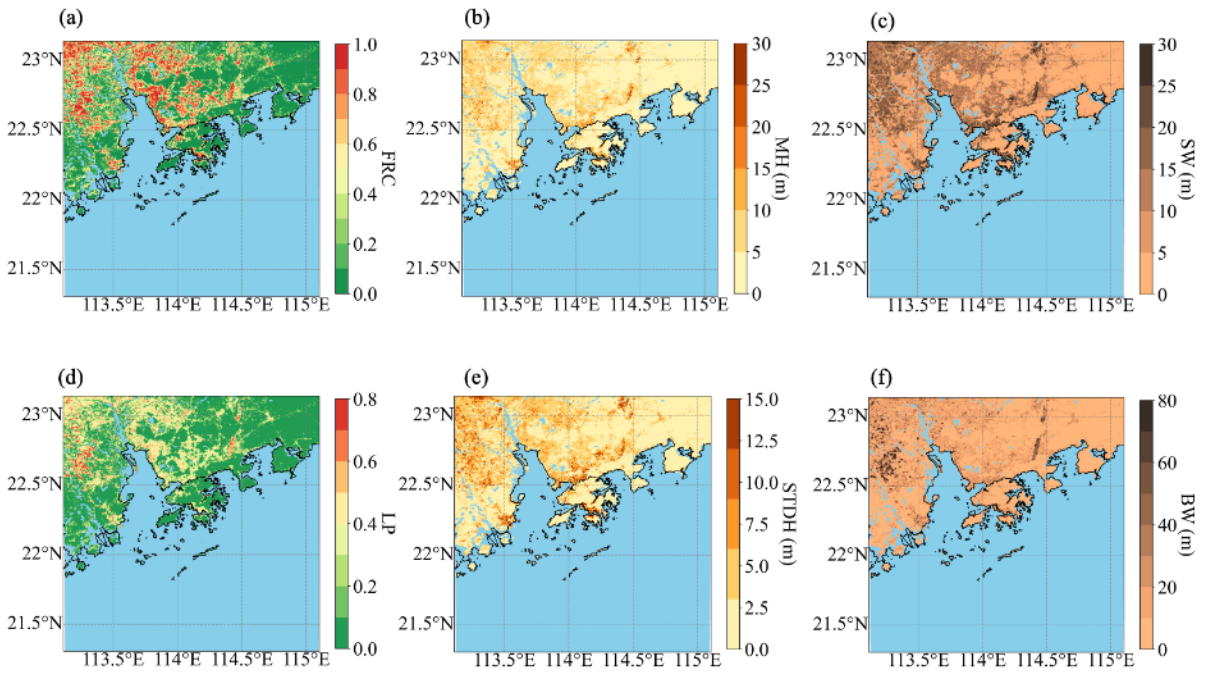

Fig. 2. Spatial distribution of (a) urban area fraction (FRC), (b) mean building height (MH), (c) street width (SW), (d) plan area fraction (LP), (e) standard deviation of building height (STDH), and (f) building width (BW) in the WRF domain d04.

2.3 Vehicle heat data

Hourly gridded vehicle heat data in Hong Kong for weekdays, Saturday, and Sunday at 800 m × 800 m resolution are adopted from Zhu et al. (2017). The VH value for each grid at each time step was calculated based on the total distance vehicles have travelled inside the grid, assuming an even distribution of different vehicle types with three kinds of fuel combustion. The fuel net combustion values are 46.4, 42.8 and 50.2 $\times 10^6$ J/kg for petrol, diesel, and liquefied petroleum gas. We mapped simulation domain d04 with the VH data by getting the interpolated value at a query point equal to the value at the nearest sample grid point. Thus, at each gird in d04, a unique VH profile with 3 (weekday, Saturday, and Sunday) × 24 values is inputted to the SLUCM as a part of the sensible heat flux. Figures 3a and 3b show the spatial distribution of the weekly mean VH over Hong Kong. The grids with high VH values are concentrated at the Kowloon Peninsula and coastal area of the Hong Kong island. Figure 3c shows the temporal profile of VH in all grids and the spatial mean VH profile. Two peaks at 9 am and 7 pm local time are distinct on weekdays but are not significant on weekends, which synchronize with the

work day and off day human activities. The VH release pattern is consistent with the road network in Hong Kong, which is shown in Fig. 3d.

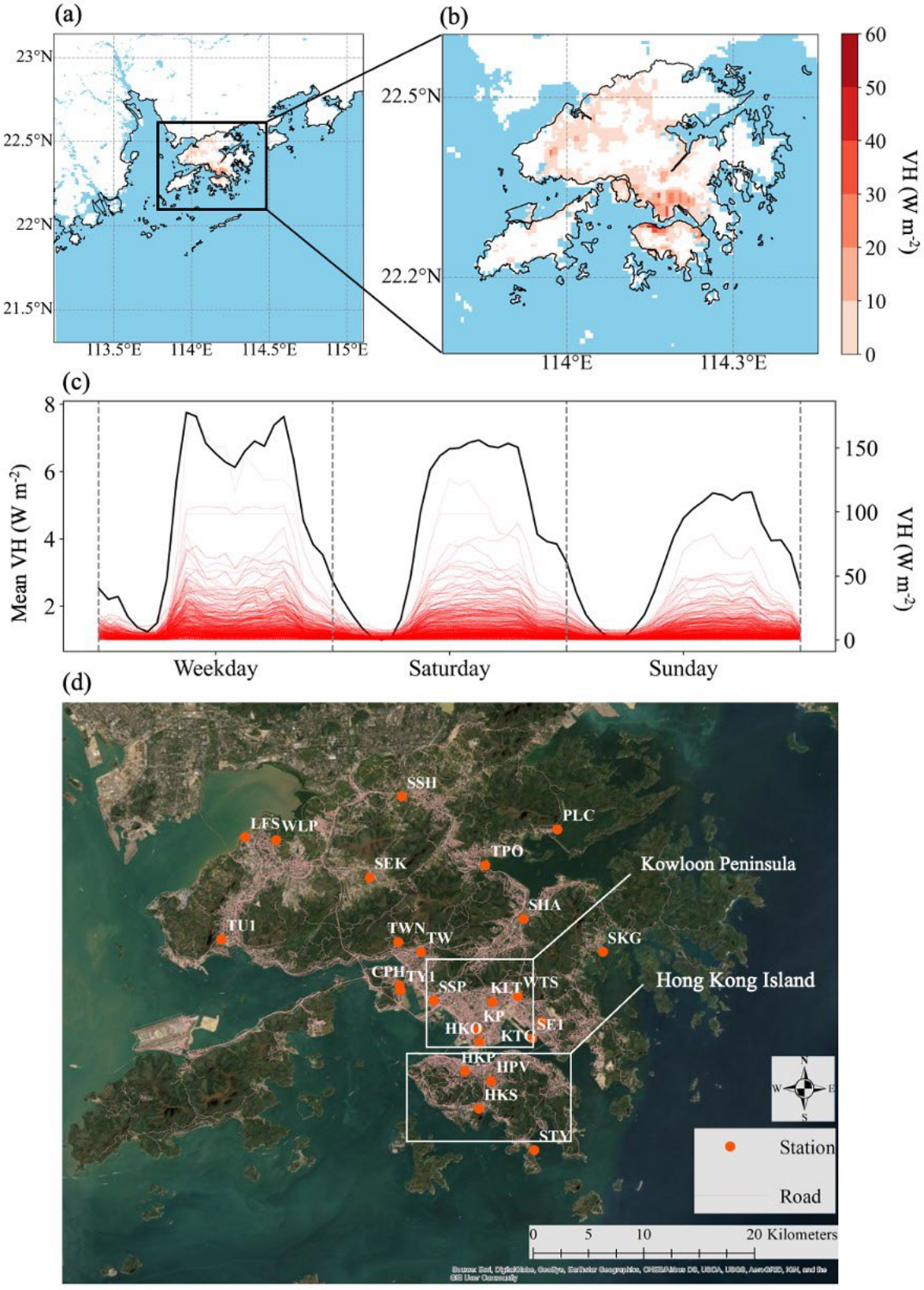

Fig. 3. (a), (b) Spatial distribution of the weekly mean VH in Hong Kong; (c) Temporal profile of VH in individual grids (red) and the spatial mean VH profile (black); (d) Road network of Hong Kong and the location of weather stations used in this study.

2.4 Numerical experiments

To investigate the seasonal variation of the impact of vehicle heat on urban thermal environment, two groups of experiments were carried out for July (summer) and January (winter) 2015. Each group contains two simulation scenarios: The control (CTRL) case without VH and the vehicle heat (VH) case with spatiotemporal VH profiles. In Hong Kong, building waste heat is important in summer but not in winter (Wang et al., 2018; Yik et al., 2001). We thus added an anthropogenic heat profile to represent the building waste heat in the summer simulations, using the prescribed profile in WRF with a peak value of 50 W m^{-2}. The accuracy of the default anthropogenic heat profile has been widely evaluated in international cities (Krayenhoff et al., 2018; Sailor et al., 2015). The simulation periods were from 1st July 00:00 (UTC) to 15th July 00:00 (UTC) 2015 and from 1st January 00:00 (UTC) to 15th January 00:00 (UTC) 2015. The first day was treated as the spin-up time, and the subsequent analyses focused on 4 weeks, from 2nd July (Thursday) to 15th July (Wednesday) in summer and from 2nd January (Friday) to 15th January (Saturday) in winter.

2.5 Weather observation data

The hourly air temperature from 24 ground-based weather stations was collected from the Hong Kong Observatory for year 2015. All stations have data quality check and the amount of missing data is < 5%. The location and ID of the stations are shown in Fig. 3d. The accuracy of simulated air temperature (T_2) was evaluated through comparisons against the measured air temperature at these stations. Statistical indicators, including root mean square error (RMSE), mean bias error (MBE) and mean absolute error (MAE) were calculated as below:

$$\mathrm{RMSE} = \sqrt{\frac{1}{\mathrm{N}}\sum_{n=1}^{\mathrm{N}}(P_n - O_n)^2}, \tag{1}$$

$$\mathrm{MBE} = \frac{1}{N}\sum_{\mathrm{n}=1}^{\mathrm{N}}(P_n - O_n), \tag{2}$$

$$\mathrm{MAE} = \left|\frac{1}{N}\sum_{\mathrm{n}=1}^{\mathrm{N}}(P_n - O_n)\right|, \tag{3}$$

where P_n is the predicted value from the WRF simulations and O_n is the observed value, n represents each time step and N is equal to the total time step.

2.6 Revised scheme for canyon air temperature

One important objective of this study is to quantify the VH impact on urban thermal environment, i.e., temperature inside street canyons. However, the standard canyon air temperature output by SLUCM is calculated from the surface temperatures of the road and the walls, which acts as an effective skin temperature of the urban canyon. And this method does not directly link canyon air temperature with the anthropogenic heat. Thus, we adopted a revised scheme proposed by Theeuwes et al. (2014) to compute canyon air temperature to ensure a meaningful VH impact estimation. The new canyon air temperature (T_2^{urb}) considers the heat exchange between the urban canyon and the overlying atmosphere, and the stability condition in the canyon:

$$T_2^{urb} = T_a + \frac{H_c r_{ah}}{\rho C_p}, \quad (4)$$

where T_a is the air temperature at the lowest atmospheric level; H_c is the sensible heat flux from the urban canyon to the overlying atmosphere; r_{ah} is the aerodynamic resistance; ρ is the air density; and C_p is the specific heat capacity of dry air. Note that estimated T_2^{urb} from this revised scheme is sensitive to the friction velocity because of the dependence of r_{ah} on stability conditon. During the winter simulation period with extremely strong winds, the scheme could predict unreasonable air temperatures at night. The abnormal values nevertheless compose less than 1% of the simulated temperature data over Hong Kong and are excluded in subsequent analysis.

2.7 Significance test

Due to the inherent uncertainty of climate simulations and background meteorological influences, significance testing is an essential method for ensuring the high possibility of the differences exist in simulated urban canyon air temperature (T_2^{urb}) between the CTRL case and VH case (Gnedenko et al., 2014). The significant test allows the investigation of locations that are likely to experience a warmer environment due to VH. Here we adopted the T-test at the 0.1 level (90% significance level) to check the significance of the temperature changes. The diurnal cycle was separated into 8 time periods, with the first period from 8 am to 10 am and the last period from 5 am to 7 am. The data of all time steps in each period were included in the significance test. One significance test was carried out for each time period separately, and it covered all grids over the innermost domain d04.

3. Results and discussions

3.1 Model evaluation

Figure 4 shows the temporal evaluation results for the WRF simulation in July and January. The hourly values of the root mean square error (RMSE) shown in Fig. 4 are the average RMSE values at 24 stations (see Fig. 3d) over Hong Kong. The RMSE is smaller in summer than in winter. The mean RMSE for T_2 during whole study period is 1.73 °C for the CTRL case and 1.82 °C for the VH case in summer, which increases to 2.54 °C and 2.58 °C in winter, respectively. The results suggest that a detailed VH profile cannot substantially improve the simulation accuracy of air temperatures over Hong Kong. Note that the RMSE here is comparable with previous studies, which focused on short periods or/and based on a few weather stations (typically 1 urban site and 1 rural site). For example, Wang et al. (2017) reported a RMSE of about 1.5 °C at 2 weather stations during their 3-days simulation over Hong Kong. Given the large number of stations used in this study, the accuracy of the weather simulations is acceptable.

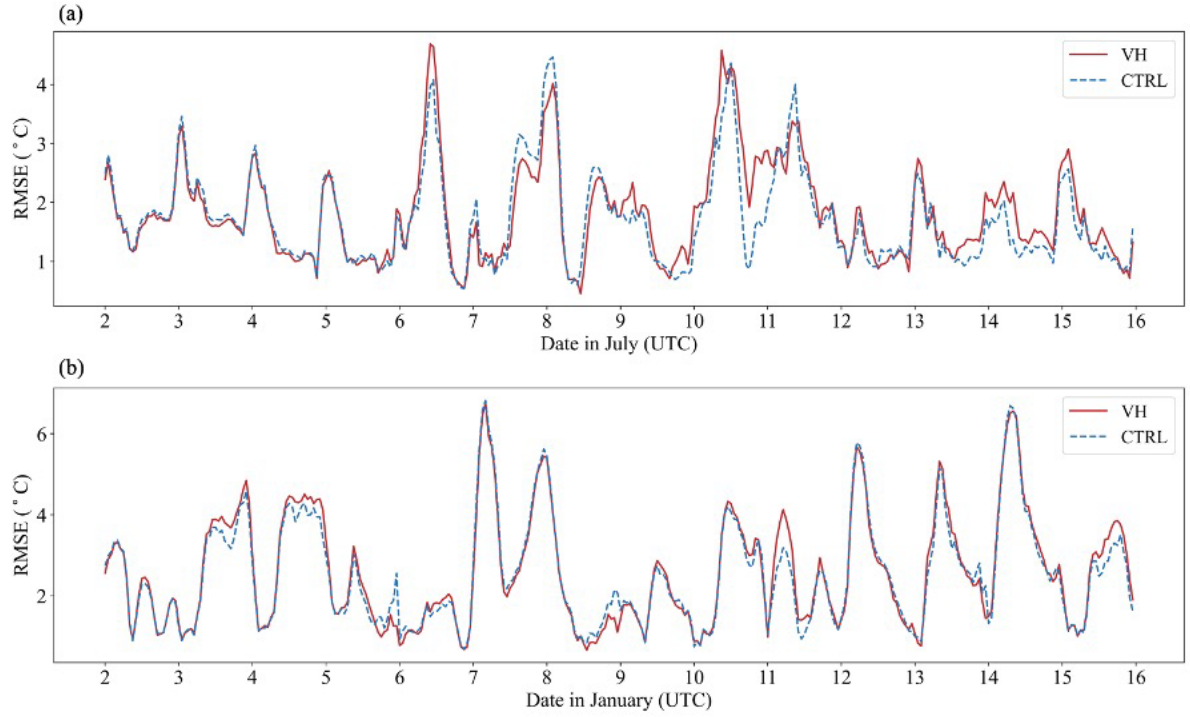

Fig. 4. Temporal variation of mean root mean square error (RMSE) for 2-m air temperature T_2 over Hong Kong in (a) summer and (b) winter.

Figures 5a and 5b show the temporal average values of MBE in the CTRL case for individual weather stations in summer and winter, respectively. The negative values in blue indicate a model underestimation, and the positive values in red represents a model overestimation. WRF

simulations tend to underestimate T_2 in summer (Fig. 5a), with the average MBE for all stations around -0.53 °C. This underestimation is more evident in the highly urbanized area. For example, the temporal mean MBE is about -1.1 °C for SSP and WTS stations located in areas with large urban area fractions. The mean MBE value for all stations is 0.42 °C during winter, and tend to be larger in the low urbanized areas. Only two stations located near compact high rise regions, HPV and HKP stations, have negative mean MBE values during winter. The result is consistent with previous findings that WRF simulations tend to overestimate rural temperatures and underestimate urban temperatures (Li et al., 2019; Zhang et al., 2016). Figures 5c and 5d show the differences of mean absolute error (ΔMAE) between the VH case and CTRL case ($\Delta MAE = MAE_{VH} - MAE_{CTRL}$). As the MAE represents the deviation of the simulated temperature from the observed temperature, negative ΔMAE values indicate improved T_2 simulations after incorporating VH profiles. During summer, implementing the VH profile improves the model accuracy at 16 stations out of 24, which are concentrated in highly urbanized areas. During the winter simulation period, the VH profile only improves the accuracy at 9 stations. The temporal mean MBE values for all stations nevertheless are between -2 to 2 °C, indicating an overall reasonable accuracy of the WRF simulations.

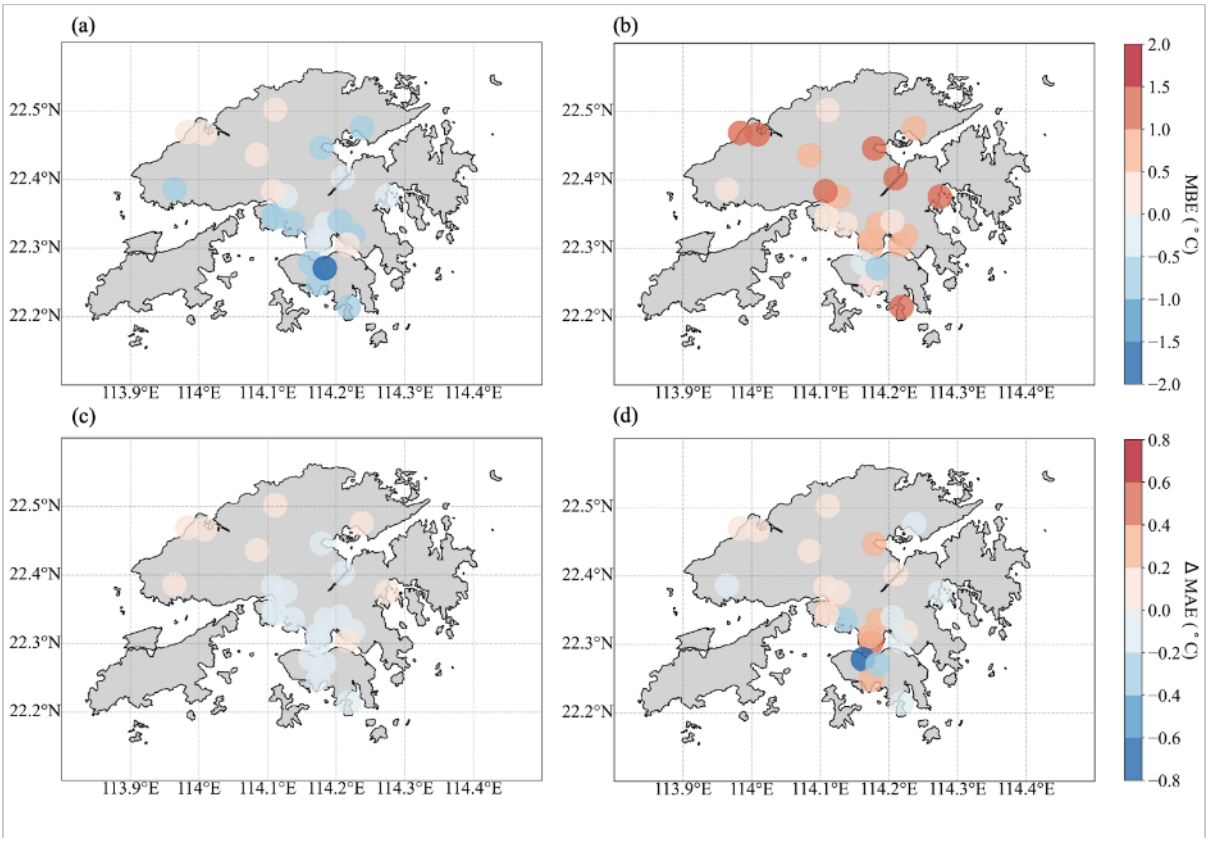

Fig. 5. Temporal average error in simulated T_2 in the CTRL case at individual weather stations: (a) mean bias error (MBE) in summer, (b) MBE in winter, (c) differences of the mean absolute error ($\Delta MAE = MAE_{VH} - MAE_{CTRL}$) in summer, and (d) ΔMAE in winter.

3.2 Temporal variation of VH impact

To study the temporal variation of the impact of vehicle heat during weekdays, Saturday and Sunday, we check the difference in the urban sensible heat flux (ΔSH^{urb}), and urban canyon air temperature (ΔT_2^{urb}) between the VH case and CTRL case. To reduce the noise introduced by small perturbations in the climate simulations, for each time step, we only include grids with VH values larger than 5 W m^{-2} into the analysis. In Hong Kong, daytime starts from 6 am and ends at 7 pm in the summer, and starts from 7 am and ends at 6 pm in the winter. The grey (white) color represents the nighttime (daytime) period in Fig. 6. Figures 6a and 6b show the impact of VH on ΔSH^{urb} in summer and winter separately. During weekdays, the largest ΔSH^{urb} occurs at 9 am and 7 pm and the lowest value is observed at 2 am, which is consistent with the VH profile in Fig. 3c. Standard deviation during daytime is found to be larger than that during nighttime. The mean ΔSH^{urb} for 2-week simulation period is 24.13 W m^{-2} during summer and 22.79 W m^{-2} during winter. And it is clear that the summer standard deviations are larger than the winter ones. Summer weather in Hong Kong is more unstable than winter weather, with heavy precipitation, strong monsoon, and notable land-sea breeze (Chen et al., 2014; Li et al., 2018; Zhou et al., 2019). The changes in regional atmospheric forcing disturb the urban thermal environment and contribute to the large variation of VH impact in summer.

By modifying SH^{urb}, VH releases in the urban area lead to changes in urban canyon air temperature (ΔT_2^{urb}) (Figs. 6c and 6d). After adding VH, the simulated 2-week mean T_2^{urb} increases by 0.21 °C in summer and by 0.35 °C in winter. The mean and standard deviation of ΔT_2^{urb} are larger in winter than in summer. One important reason is that the same amount of VH becomes a larger part of the total sensible heat flux during winter as the natural radiation level decreases (Fan & Sailor, 2005). Another plausible reason may be the strong land-sea breezes during summer spread VH from the releasing places to surrounding areas quickly (Wang et al., 2015; Zhou et al., 2019). Despite the positive VH, negative values of ΔT_2^{urb} could occur at weekends during daytime, especially on Sundays with low traffic flow and small VH. Results here demonstrate that the VH impact varies with time notably at the daily scale and

seasonal sacle. It is worth mentioning that the temporal analysis in this section only includes areas with considerable VH emission (> 5 W m^{-2}). The time series results only illustrate partial effects of VH, as VH releases could also modify surrounding rural areas. Thus, spatial analysis with significance test is conducted next to investigate the spatial variation of VH impact.

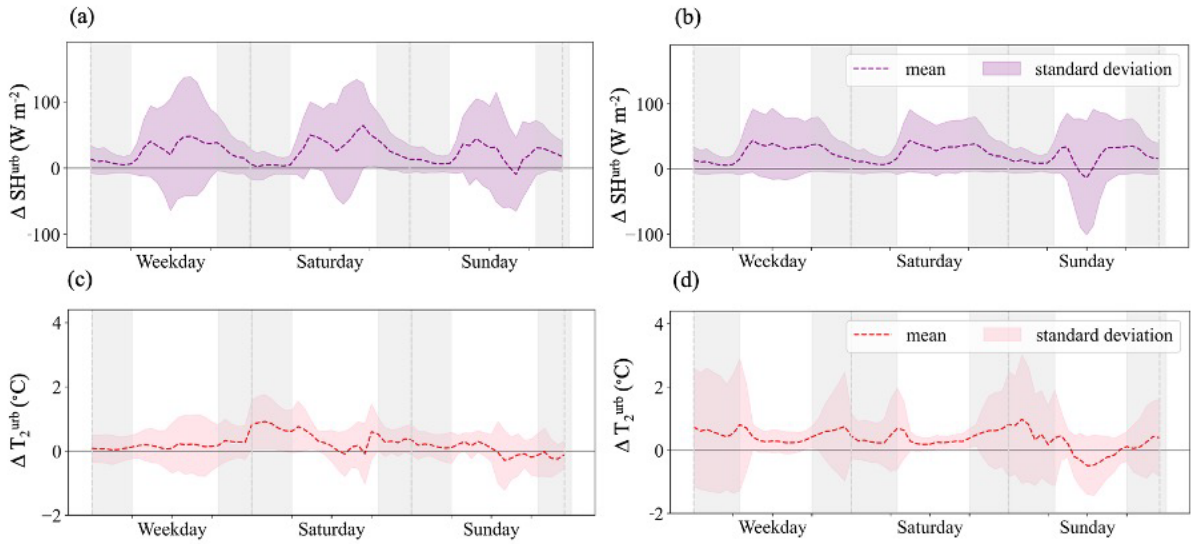

Fig. 6. Differences of urban sensible heat flux (ΔSH^{urb}), and urban canyon air temperature (ΔT_2^{urb}) between the VH case and CTRL case (a), (c) in summer and (b), (d) in winter. The dash lines represent the mean profiles and the shaded areas represent one standard deviation away from the mean.

3.3 Spatial variation of VH impact

Figures 7 and 8 show the spatial distribution of ΔT_2^{urb} over Hong Kong in summer and winter, respectively. Figures 7a to 7h represent 8 different time periods throughout the diurnal cycle. Because of the rush hours around 9 am and 7 pm, the strongest VH impact is found during the first time period (Figs. 7a and 8a) and the fourth time period (Figs. 7a and 8d). In summer, VH emissions increase T_2^{urb} over most land areas (positive ΔT_2^{urb}) from late night to early morning (Figs. 7f-h and 7a). During 5 am – 7am, around 97.5% of the Hong Kong land area experiences a higher urban canyon air temperature, with a spatial mean of 0.12 °C. In the mid of the day and late afternoon, however, decreased T_2^{urb} by VH is found over a large spatial extent. For example, during 5 pm – 7 pm, about 63.0% of the land area has a lower temperature and the spatial mean impact of VH over entire Hong Kong is -0.03 °C. The negative spatial mean is mainly caused by temperature reductions over the southwestern part, which may due to the strong see breeze in summer. Despite the negative spatial mean ΔT_2^{urb}, the strong VH at

daytime results in the higher T_2^{urb} in densely urbanized area. The Kowloon Peninsula and the northern part of the Hong Kong island, representing the most urbanized areas in Hong Kong, have a ΔT_2^{urb} of more than 1 °C from 2 pm to 7 pm. The VH impact on urban canyon air temperature is more noticeable in winter. In winter, the release of VH consistently increase T_2^{urb} across the Hong Kong land area during all the periods. The largest spatial mean ΔT_2^{urb} of 0.16 °C occurs during 11 pm – 1 am. Figures 8e and 8f show strong VH impacts over the low-density urbanized area with highways in the northern part of Hong Kong during 8pm – 1am. This proves that where VH is the only contributor of the anthropogenic heat, it can be a major factor for the winter nighttime warming at neighbourhoods with large traffic flow.

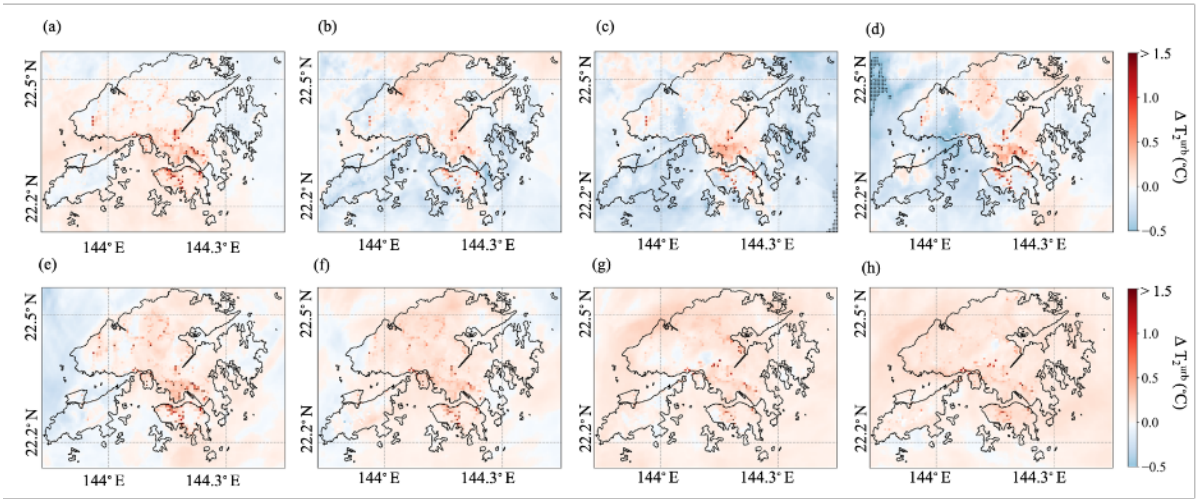

Fig. 7. Spatial distribution of the mean difference in urban canyon air temperature (ΔT_2^{urb}) between VH and CTRL cases over Hong Kong in summer: (a) 8 am – 10am, (b) 11 am – 1 pm, (c) 2 pm – 4 pm, (d) 5 pm – 7 pm, (e) 8 pm – 10 pm, (f) 11 pm – 1 am, (g) 2 am – 4 am, (h) 5 am – 7am. Dotted areas stand for regions with impacts statistically significant at the 0.1 level.

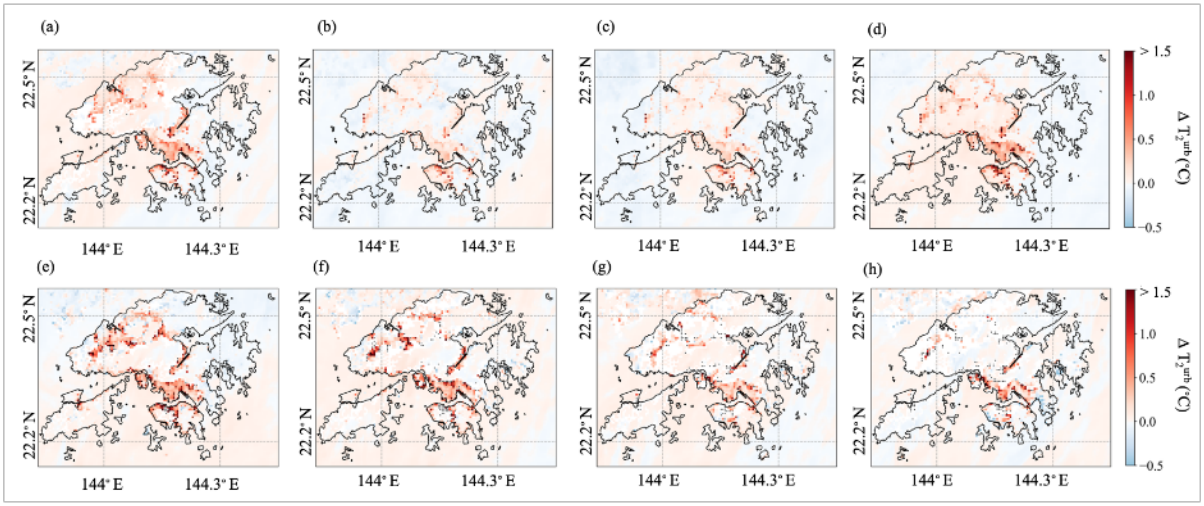

Fig. 8. Same as Fig. 7, but for winter.

The dotted areas in Figs. 7 and 8 represent regions where VH-induced temperature changes are statistically significant at the 90% confidence level. In summer, all the dotted areas have positive ΔT_2^{urb}. The largest ΔT_2^{urb} by VH is found during the morning rush hours (8 am – 10 am), with a spatial mean of 0.89 °C over the significant grids. During 8 pm – 10 pm, a total of 21 km^2 land area has significant higher T_2^{urb} due to the release of VH, and the maximum ΔT_2^{urb} can reach 1.57 °C. In winter, the spatial mean of ΔT_2^{urb} over the significant grids is at least about 1.0 °C at different periods throughout the day. During nighttime and rush hours, large area with significant ΔT_2^{urb} values are found among the highly urbanized regions. Between 8 am and 10 am on winter days, the VH can affect 8.75 km^2 area with an 1.23 °C significantly higher T_2^{urb} on average. During the 5th period (8 pm – 10 pm) in winter, 38.25 km^2 area exposes to an 1.08 °C mean significant ΔT_2^{urb} and can reach 2.59 °C in maximum. Note that the significant VH impact on T_2^{urb} has the widest spatial coverage during 8 pm – 10 pm in both summer and winter. This large impact shortly after sunset can be explained by: 1) strong VH releases at the afternoon rush hour 7 pm spread to nearby areas; 2) the stored VH by engineering materials during daytime starts to be released into the city as the solar radiation decreases rapidly.

3.4 Relationship between VH impact and urban morphology

To diagnose the VH impact on thermal environment in different urban neighbourhoods, we examine the relationship between the VH impact and urban morphology in this section. Figure 9 shows the distribution of ΔT_2^{urb} over different ranges of the three urban morphology parameters (urban area fraction, mean building height and the aspect ratio) during one daytime period (8 am – 10 am) and one nighttime period (11 pm – 1 am) in summer. A general increasing trend is found between ΔT_2^{urb} and FRC, and between ΔT_2^{urb} and MH. For highly urbanized regions with 0.8 – 1.0 FRC, mean ΔT_2^{urb} is around 0.12 °C in the morning (Fig. 9a) and around 0.16 °C at night (Fig. 9d). Neighbourhoods with tall buildings (> 24 m) have 0.11 °C higher ΔT_2^{urb} than those with 0 – 6 m buildings (Figs. 9b and 9e). Note that the box plots exclude the outliers that the maximum values are slightly different in three figures for the same period.

Positive relationships between ΔT_2^{urb} and FRC/MH over entire Hong Kong are also found in winter. Figure 10 shows that ΔT_2^{urb} by vehicle heat is much larger in highly urbanized

neighbourhoods and in areas with high-rise buildings in winter than in summer. Compared to the ΔT_2^{urb} of 0.05 °C in regions with FRC of 0 – 0.2, the areas with FRC of 0.8 – 1.0 has a mean ΔT_2^{urb} of 0.29 °C during the morning rush hour (Fig. 10a) and 0.39 °C at night (Fig. 10d). Neighbourhoods with tall buildings (> 24 m) experience the strongest VH impact, with mean ΔT_2^{urb} of 0.62 °C at night between 11 pm and 1 am. On the other hand, VH-induced ΔT_2^{urb} does not have a clear relationship with the aspect ratio (Figs. 9c, 9f, 10c and 10f), which indicates the compactness of a neighbourhood. Maximum ΔT_2^{urb} are found over neighbourhoods with MH/SW in the range of 0.4 – 0.6 in winter. The magnitude of VH and urban morphology jointly influence the neighbourhood thermal environment. Tall buildings reduce the air ventilation and subsequent dispersion of anthropogenic heat that high-rise neighbourhoods can strengthen urban nighttime warming, as pointed out in previous studies (Wang et al., 2018; Yuan et al., 2020). Meanwhile, vehicle heat emission depends on the traffic density on roads that wide streets tend to have notable VH. This is one reason that ΔT_2^{urb} has a strong relationship with the mean building height but not with the aspect ratio.

The distributions of the significant ΔT_2^{urb} are different from the ΔT_2^{urb} over the whole land area in Hong Kong. The significant ΔT_2^{urb} means the area has a high possibility to experience a warmer environment throughout the whole study period due to VH. During the morning rush hours, most of the grids with significant ΔT_2^{urb} belong to the lowest FRC group (0 – 0.2), and the mean significant ΔT_2^{urb} reaches 0.93 °C and 1.24 °C in summer (Fig. 9g) and winter (Fig. 10g), respectively. A similar pattern is found in summer nights (Fig. 9j) but not in winter nights (Fig. 10j). In winter, highly urbanized areas with FRC of 0.6 – 1.0 have mean ΔT_2^{urb} around 1.19 °C, which is greater than areas with low FRC. In terms of mean building height, ΔT_2^{urb} is prominent in neighbourhoods with the lowest and highest buildings. The mean significant ΔT_2^{urb} is 1.13 °C for the 0 – 6 m MH group and is 1.24 °C for the > 24 m MH group in simulated winter nights (Fig. 10k). The major reason is that the VH is released along the roads, and many highways and city circulation roads with large traffic flow are located in low urbanized areas in Hong Kong, such as along the seashore or near mountains. On the other hand, part of highly urbanized neighbourhoods or/and high-rise building area are downtown areas with dense traffic, where the VH can be trapped among the buildings. On winter nights, the impact of VH on urban thermal environment becomes more noticeable and results in the highest mean significant ΔT_2^{urb} compared to other studied periods. The relationship between significant

ΔT_2^{urb} and aspect ratio is not as notable as those between significant ΔT_2^{urb} and FRC/MH. This finding is consistent with the results over the whole land area in Hong Kong.

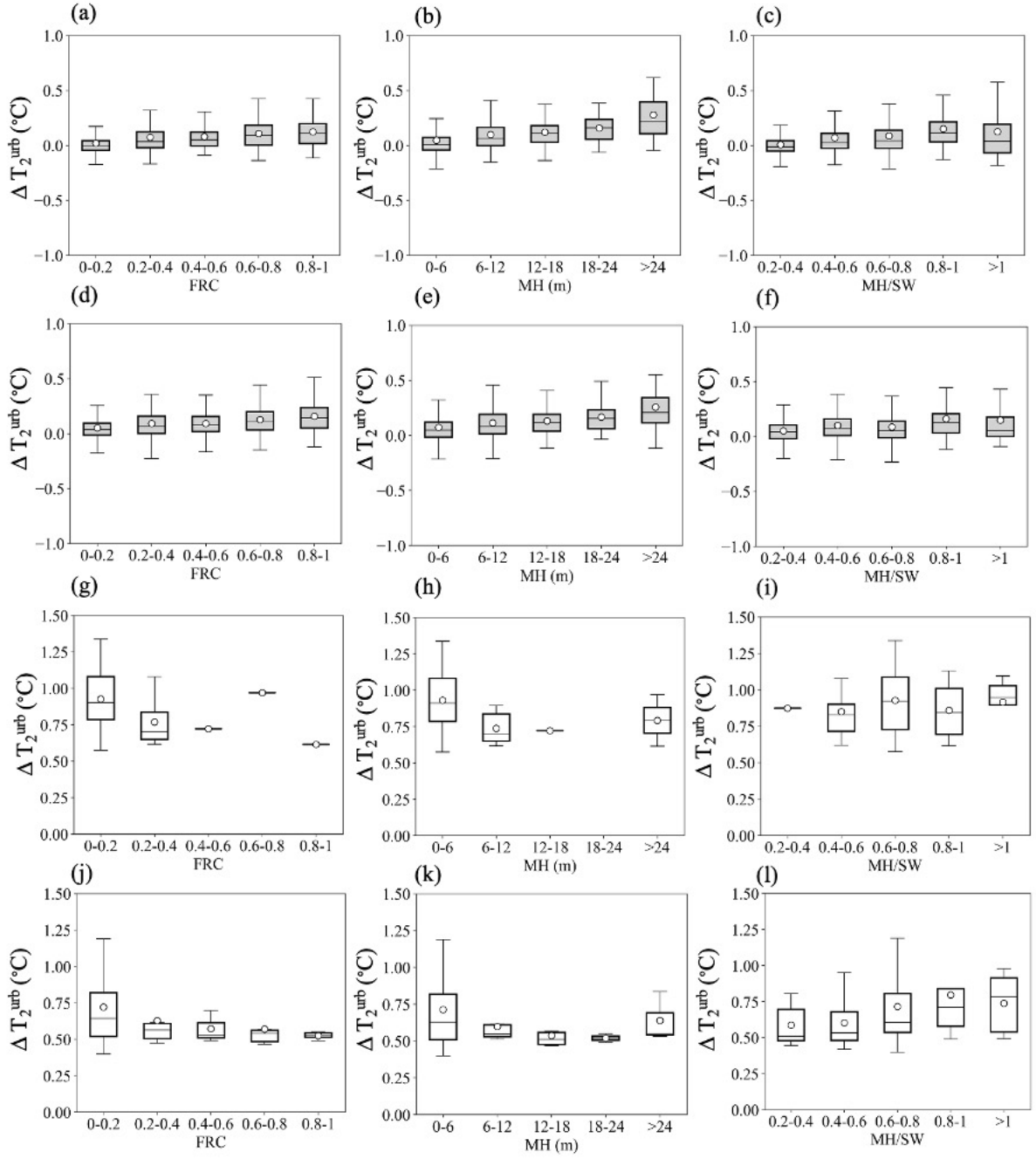

Fig. 9. Distribution of ΔT_2^{urb} in Hong Kong land area over different ranges of (a) urban area fraction (FRC), (b) mean building height (MH), and (c) the aspect ratio (MH/SW) during the morning rush hour (8 am – 10 am). (d)-(f) Same as (a)-(c) but for 11 pm – 1 am. (g)-(l) Same as (a)-(f) but for the grids with significant ΔT_2^{urb} at the 90% confident level. The upper and lower bars of each box are the maximum and minimum values excluding the ottrelite. The bar in the middle of each box represents the medium value and the circle represents the mean value.

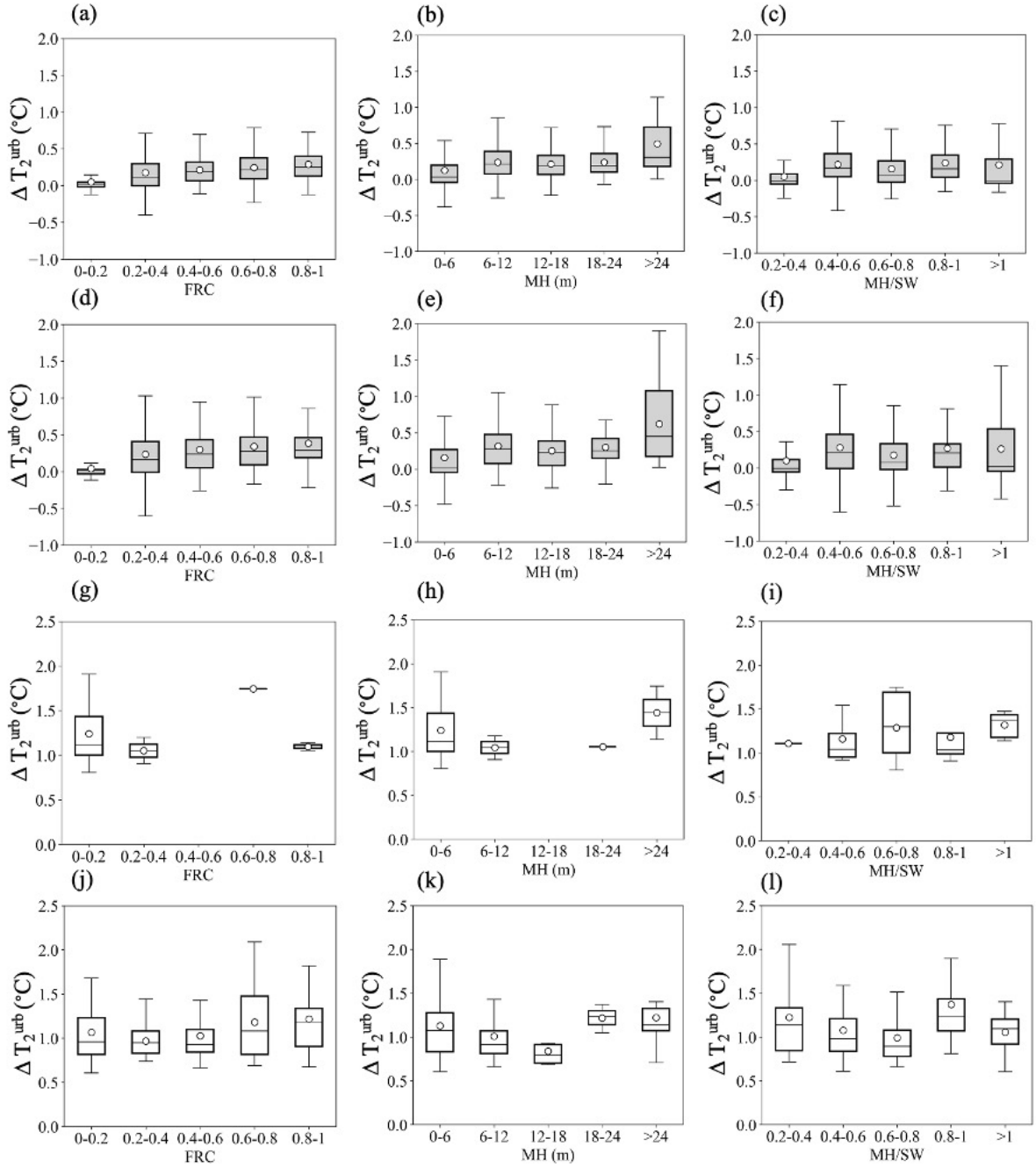

Fig. 10. Same as Fig. 9, but for winter.

4. Conclusions

In this paper, we quantify the spatiotemporal effect of vehicle heat on the thermal environment of Hong Kong using the coupled WRF-SLUCM modelling system. Results show that VH emissions have a more substantial impact on the urban canyon air temperature (T_2^{urb}) in weekdays than over weekends. Strong seasonal variations of the VH impact are found, where

the simulated 2-week mean T_2^{urb} increases by 0.35 °C in winter and by 0.21 °C in summer. The VH impact on thermal environment has large spatial variations that negative temperature changes are found over some land areas during daytime. Yet, highly urbanized regions in Hong Kong consistently experience a warmer thermal environment, especially in the rush hours and at night. The significance test is a valuable measure for distinguishing the areas significantly modified by the VH. In both summer and winter, the statistically significant VH impact on T_2^{urb} has the widest spatial extent during 8 pm – 10 pm. Over land areas in Hong Kong, VH impact is found to increase with urban area fraction and mean building height. However, the areas with statistically significant VH impacts are mainly low urbanized regions with large traffic flows and densely built-up regions with high-rise building. The relationship between the VH impact and canyon aspect ratio is inconclusive.

It is noteworthy that this study incorporates fine-resolution VH and urban landscape data into weather simulations. As a result, the warming effect by vehicle heat is found to be larger than those reported in previous studies on AH in Hong Kong (Feng et al., 2012; Zhang et al., 2016). The VH could synergistically interact with building waste heat and further aggravate the microclimatic conditions in Hong Kong. Modelling building waste heat in urban climate simulations nevertheless requires the development of building energy parameterizations for the single-layer urban canopy model, which is beyond the score of this study. One limitation of the present study is that the impact of VH is only investigated through canyon air temperature. The humidity and wind speed can also be affected by the VH. Previous studies pointed out that AH can make the built environment drier (Feng et al., 2012; Zhang et al., 2016), and modify the potential temperature profiles in the planetary boundary layer (Nie et al., 2017). Future studies may explore the impact of vehicle heat on these aspects.

A higher urban canyon air temperature due to the VH could increase the population exposure to heat stress in Hong Kong, especially during rush hours. And thus the VH impact has implications for population behaviours and social policies related to health risk. Quantifying the impact of vehicle heat is important given the global trend of electrifying vehicles (World Energy Outlook 2019, Ivanchev & Fonseca, 2020; Singh et al., 2020). Though the absolute magnitude would change from city to city, our study provides a good estimation of the VH impact on canyon air temperature in one of the most densely populated cities. Because of the positive feedback between the temperature and energy demands (Kikegawa et al., 2003;

Takane et al., 2019), potential benefits in energy saving by reducing the VH can be of interests in future studies.

Acknowledgements

This work was supported by the Hong Kong Research Grants Council funded project 26202319. The numerical simulation for this article was supported by the supercomputer services at the National Tianhe-2 center in Guangzhou, P.R. China.

References

Allen, L., Lindberg, F., & Grimmond, C. S. B. (2011). Global to city scale urban anthropogenic heat flux: Model and variability. *International Journal of Climatology*, *31*(13), 1990–2005. https://doi.org/10.1002/joc.2210

Block, A., Keuler, K., & Schaller, E. (2004). Impacts of anthropogenic heat on regional climate patterns. *Geophysical Research Letters*, *31*(12). https://doi.org/10.1029/2004GL019852

Bohnenstengel, S. I., Hamilton, I., Davies, M., & Belcher, S. E. (2014). Impact of anthropogenic heat emissions on London's temperatures. *Quarterly Journal of the Royal Meteorological Society, 140*(679), 687–698. https://doi.org/10.1002/qj.2144

Cai, M., Shi, Y., & Ren, C. (2020). Developing a high-resolution emission inventory tool for low-carbon city management using hybrid method – A pilot test in high-density Hong Kong. *Energy and Buildings*, *226*, 110376. https://doi.org/10.1016/j.enbuild.2020.110376

Chen, F, & Dudhia, J. (2001). Coupling an advanced land surface-hydrology model with the Penn State-NCAR MM5 modeling system. Part I. Model implementation and sensitivity. *Monthly Weather Review*, 569–585.

Chen, F, Yang, X., & Wu, J. (2016). Simulation of the urban climate in a Chinese megacity with spatially heterogeneous anthropogenic heat data. *Journal of Geophysical Research: Atmospheres*, *121*(10), 5193–5212. https://doi.org/10.1002/2015JD024642

Chen, X, Zhao, K., & Xue, M. (2014). Spatial and temporal characteristics of warm season convection over Pearl River Delta region, China, based on 3 years of operational radar data. *Journal of Geophysical Research: Atmospheres*, *119*(22), 12,447-12,465. https://doi.org/10.1002/2014JD021965

Chen, X. & Jeong, S.-J. (2018). Shifting the urban heat island clock in a megacity: A case study of Hong Kong. *Environmental Research Letters*, *13*(1), 014014. https://doi.org/10.1088/1748-9326/aa95fb

Chow, W. T. L., Salamanca, F., Georgescu, M., Mahalov, A., Milne, J. M., & Ruddell, B. L. (2014). A multi-method and multi-scale approach for estimating city-wide anthropogenic heat fluxes. *Atmospheric Environment*, *99*, 64–76. https://doi.org/10.1016/j.atmosenv.2014.09.053

Dudhia, J. (1989). Numerical study of convection observed during the winter monsoon experiment using a mesoscale two-dimensional model. *Journal of Atmospheric Sciences*, *46*(20), 3077-3107. https://doi.org/10.1175/1520-0469(1989)046<3077:NSOCOD>2.0.CO;2

Fan, H., & Sailor, D. J. (2005). Modeling the impacts of anthropogenic heating on the urban climate of Philadelphia: A comparison of implementations in two PBL schemes. *Atmospheric Environment*, *39*(1), 73–84. https://doi.org/10.1016/j.atmosenv.2004.09.031

Feng, J. M., Wang, Y. L., Ma, Z. G., & Liu, Y. H. (2012). Simulating the regional impacts of urbanization and anthropogenic heat release on climate across China. *Journal of Climate*, *25*(20), 7187-7203. https://doi.org/10.1175/JCLI-D-11-00333.1

Ferreira, M. J., de Oliveira, A. P., & Soares, J. (2011). Anthropogenic heat in the city of São Paulo, Brazil. *Theoretical and Applied Climatology*, *104*(1), 43–56. https://doi.org/10.1007/s00704-010-0322-7

Gago, E. J., Roldan, J., Pacheco-Torres, R., & Ordóñez, J. (2013). The city and urban heat islands: A review of strategies to mitigate adverse effects. *Renewable and Sustainable Energy Reviews*, *25*, 749–758. https://doi.org/10.1016/j.rser.2013.05.057

Gnedenko, B. V., Belyayev, Y. K., & Solovyev, A. D. (2014). *Mathematical Methods of Reliability Theory*. Academic Press.

Hong, S. Y., & Lim, J. O. J. (2006). The WRF single-moment 6-class microphysics scheme (WSM6). *Asia-Pacific Journal of Atmospheric Sciences*, *42*(2), 129-151.

Iamarino, M., Beevers, S., & Grimmond, C. S. B. (2012). High-resolution (space, time) anthropogenic heat emissions: London 1970–2025. *International Journal of Climatology*, *32*(11), 1754–1767. https://doi.org/10.1002/joc.2390

Ivanchev, J., & Fonseca, J. A. (2020). *Anthropogenic heat due to road transport: a mesoscopic assessment and mitigation potential of electric vehicles and autonomous vehicles in Singapore* (pp. D1-2). ETH Zurich. https://doi.org/10.3929/ethz-b-000401288

Janjić, Z. I. (1994). The step-mountain eta coordinate model: Further developments of the convection, viscous sublayer, and turbulence closure schemes. *Monthly weather review*, *122*(5), 927-945. https://doi.org/10.1175/1520-0493(1994)122<0927:TSMECM>2.0.CO;2

Kikegawa, Y., Genchi, Y., Yoshikado, H., & Kondo, H. (2003). Development of a numerical simulation system toward comprehensive assessments of urban warming countermeasures including their impacts upon the urban buildings' energy-demands. *Applied Energy*, *76*(4), 449–466. https://doi.org/10.1016/S0306-2619(03)00009-6

Krayenhoff, E. S., Moustaoui, M., Broadbent, A. M., Gupta, V., & Georgescu, M. (2018). Diurnal interaction between urban expansion, climate change and adaptation in US cities. *Nature Climate Change*, *8*(12), 1097–1103. https://doi.org/10.1038/s41558-018-0320-9

Kusaka, H., Kondo, H., Kikegawa, Y., & Kimura, F. (2001). A simple single-layer urban canopy model for atmospheric models: Comparison with multi-layer and slab

models. *Boundary-layer meteorology*, *101*(3), 329-358. https://doi.org/10.1023/A:1019207923078

Li, D., & Bou-Zeid, E. (2013). Synergistic interactions between urban heat islands and heat waves: The impact in cities is larger than the sum of its parts. *Journal of Applied Meteorology and Climatology*, *52*(9), 2051-2064. https://doi.org/10.1175/JAMC-D-13-02.1

Li, H., Zhou, Y., Wang, X., Zhou, X., Zhang, H., & Sodoudi, S. (2019). Quantifying urban heat island intensity and its physical mechanism using WRF/UCM. *Science of The Total Environment*, *650*, 3110–3119. https://doi.org/10.1016/j.scitotenv.2018.10.025

Li, X., Lau, N. C., & Lee, T. C. (2018). An observational study of the diurnal variation of precipitation over Hong Kong and the underlying processes. *Journal of Applied Meteorology and Climatology*, *57*(6), 1385-1402. https://doi.org/10.1175/JAMC-D-17-0320.1

Liu, J., Hansen, A., Varghese, B., Liu, Z., Tong, M., Qiu, H., Tian, L., Lau, K. K.-L., Ng, E., Ren, C., & Bi, P. (2020). Cause-specific mortality attributable to cold and hot ambient temperatures in Hong Kong: A time-series study, 2006–2016. *Sustainable Cities and Society*, *57*, 102131. https://doi.org/10.1016/j.scs.2020.102131

Madlener, R., & Sunak, Y. (2011). Impacts of urbanization on urban structures and energy demand: What can we learn for urban energy planning and urbanization management? *Sustainable Cities and Society*, *1*(1), 45–53. https://doi.org/10.1016/j.scs.2010.08.006

Mlawer, E. J., Taubman, S. J., Brown, P. D., Iacono, M. J., & Clough, S. A. (1997). Radiative transfer for inhomogeneous atmospheres: RRTM, a validated correlated-k model for the longwave. *Journal of Geophysical Research: Atmospheres*, *102*(D14), 16663–16682. https://doi.org/10.1029/97JD00237

Molnár, G., Kovács, A., & Gál, T. (2020). How does anthropogenic heating affect the thermal environment in a medium-sized Central European city? A case study in Szeged, Hungary. *Urban Climate*, *34*, 100673. https://doi.org/10.1016/j.uclim.2020.100673

Nations, U. (2018). revision of world urbanization prospects," 2018. *United Nations Department of Economic and Social Affairs*.

Nie, W., Zaitchik, B. F., Ni, G., & Sun, T. (2017). Impacts of anthropogenic heat on summertime rainfall in Beijing. *Journal of Hydrometeorology*, *18*(3), 693-712. https://doi.org/10.1175/JHM-D-16-0173.1

Noh, Y., Cheon, W. G., Hong, S. Y., & Raasch, S. (2003). Improvement of the K-profile model for the planetary boundary layer based on large eddy simulation data. *Boundary-Layer Meteorology*, *107*(2), 401–427. Scopus. https://doi.org/10.1023/A:1022146015946

Pigeon, G., Legain, D., Durand, P., & Masson, V. (2007). Anthropogenic heat release in an old European agglomeration (Toulouse, France). *International Journal of Climatology*, *27*(14), 1969–1981. https://doi.org/10.1002/joc.1530

Quah, A. K. L., & Roth, M. (2012). Diurnal and weekly variation of anthropogenic heat emissions in a tropical city, Singapore. *Atmospheric Environment*, *46*, 92–103. https://doi.org/10.1016/j.atmosenv.2011.10.015

Ren, C., Cai, M., Li, X., Zhang, L., Wang, R., Xu, Y., & Ng, E. (2019). Assessment of local climate zone classification maps of cities in China and feasible refinements. *Scientific reports*, *9*(1), 1-11. https://doi.org/10.1038/s41598-019-55444-9

Sailor, D. J. (2011). A review of methods for estimating anthropogenic heat and moisture emissions in the urban environment. *International Journal of Climatology*, *31*(2), 189–199. https://doi.org/10.1002/joc.2106

Sailor, D. J., Georgescu, M., Milne, J. M., & Hart, M. A. (2015). Development of a national anthropogenic heating database with an extrapolation for international cities. *Atmospheric Environment*, *118*, 7–18. https://doi.org/10.1016/j.atmosenv.2015.07.016

Sailor, D. J., & Lu, L. (2004). A top–down methodology for developing diurnal and seasonal anthropogenic heating profiles for urban areas. *Atmospheric Environment*, *38*(17), 2737–2748. https://doi.org/10.1016/j.atmosenv.2004.01.034

Salamanca, F., Georgescu, M., Mahalov, A., Moustaoui, M., & Wang, M. (2014). Anthropogenic heating of the urban environment due to air conditioning. *Journal of Geophysical Research: Atmospheres*, *119*(10), 5949–5965. https://doi.org/10.1002/2013JD021225

Salvati, A., Coch Roura, H., & Cecere, C. (2017). Assessing the urban heat island and its energy impact on residential buildings in Mediterranean climate: Barcelona case study. *Energy and Buildings*, *146*, 38–54.

Santamouris, M., Papanikolaou, N., Livada, I., Koronakis, I., Georgakis, C., Argiriou, A., & Assimakopoulos, D. N. (2001). On the impact of urban climate on the energy consumption of buildings. *Solar Energy*, *70*(3), 201–216. https://doi.org/10.1016/S0038-092X(00)00095-5

Singh, V. K., Acero, J. A., & Martilli, A. (2020). Evaluation of the impact of anthropogenic heat emissions generated from road transportation and power plants on the UHI intensity of Singapore. *Technical Report Cooling Singapore*, *500*. https://doi.org/10.3929/ETHZ-B-000452434

Skamarock, W. C., Klemp, J. B., Dudhia, J., Gill, D. O., Barker, D., Duda, M. G., … Powers, J. G. (2008). *A Description of the Advanced Research WRF Version 3* (No. NCAR/TN-475+STR). University Corporation for Atmospheric Research. http://dx.doi.org/10.5065/D68S4MVH

Smith, C., Lindley, S., & Levermore, G. (2009). Estimating spatial and temporal patterns of urban anthropogenic heat fluxes for UK cities: The case of Manchester. *Theoretical and Applied Climatology*, *98*(1), 19–35. https://doi.org/10.1007/s00704-008-0086-5

Stewart, I. D., & Oke, T. R. (2012). Local climate zones for urban temperature studies. *Bulletin of the American Meteorological Society*, *93*(12), 1879-1900. https://doi.org/10.1175/BAMS-D-11-00019.1

Sun, R., Wang, Y., & Chen, L. (2018). A distributed model for quantifying temporal-spatial patterns of anthropogenic heat based on energy consumption. *Journal of Cleaner Production*, *170*, 601–609. https://doi.org/10.1016/j.jclepro.2017.09.153

Sun, Y., Hu, T., & Zhang, X. (2018). Substantial increase in heat wave risks in China in a future warmer world. *Earth's Future*, *6*(11), 1528-1538. https://doi.org/10.1029/2018EF000963

Takane, Y., Kikegawa, Y., Hara, M., & Grimmond, C. S. B. (2019). Urban warming and future air-conditioning use in an Asian megacity: Importance of positive feedback. *Npj Climate and Atmospheric Science*, *2*(1), 1-11. https://doi.org/10.1038/s41612-019-0096-2

Theeuwes, N. E., Steeneveld, G. J., Ronda, R. J., Heusinkveld, B. G., Hove, L. W. A. van, & Holtslag, A. a. M. (2014). Seasonal dependence of the urban heat island on the street canyon aspect ratio. *Quarterly Journal of the Royal Meteorological Society*, *140*(684), 2197–2210. https://doi.org/10.1002/qj.2289

Wang, Y., Li, Y., Sabatino, S. D., Martilli, A., & Chan, P. W. (2018). Effects of anthropogenic heat due to air-conditioning systems on an extreme high temperature event in Hong Kong. *Environmental Research Letters*, *13*(3), 034015. https://doi.org/10.1088/1748-9326/aaa848

Wang, Y., Sabatino, S. D., Martilli, A., Li, Y., Wong, M. S., Gutiérrez, E., & Chan, P. W. (2017). Impact of land surface heterogeneity on urban heat island circulation and sea-land breeze circulation in Hong Kong. *Journal of Geophysical Research: Atmospheres*, *122*(8), 4332–4352. https://doi.org/10.1002/2017JD026702

Wang, Yi, Li, Y., Xue, Y., Martilli, A., Shen, J., & Chan, P. W. (2020). City-scale morphological influence on diurnal urban air temperature. *Building and Environment*, *169*, 106527. https://doi.org/10.1016/j.buildenv.2019.106527

Wong, M. M. F., Fung, J. C. H., Ching, J., Yeung, P. P. S., Tse, J. W. P., Ren, C., Wang, R., & Cai, M. (2019). Evaluation of uWRF performance and modeling guidance based on

WUDAPT and NUDAPT UCP datasets for Hong Kong. *Urban Climate*, *28*, 100460. https://doi.org/10.1016/j.uclim.2019.100460

Wong, M. S., Yang, J., Nichol, J., Weng, Q., Menenti, M., & Chan, P. W. (2015). Modeling of anthropogenic heat flux using HJ-1B Chinese small satellite image: A study of heterogeneous urbanized areas in Hong Kong. *IEEE Geoscience and Remote Sensing Letters*, *12*(7), 1466-1470. https://doi.org/10.1109/LGRS.2015.2409111

World Energy Outlook 2019. (n.d.). IEA Webstore. Retrieved September 25, 2020, from https://webstore.iea.org/world-energy-outlook-2019

Yang, B., Yang, X., Leung, L. R., Zhong, S., Qian, Y., Zhao, C., ... & Qi, J. (2019). Modeling the impacts of urbanization on summer thermal comfort: the role of urban land use and anthropogenic heat. *Journal of Geophysical Research: Atmospheres*, *124*(13), 6681-6697. https://doi.org/10.1029/2018JD029829

Yang, J., & Bou-Zeid, E. (2018). Should cities embrace their heat islands as shields from extreme cold?. *Journal of Applied Meteorology and Climatology*, *57*(6), 1309-1320. https://doi.org/10.1175/JAMC-D-17-0265.1

Yang, J., Wang, Z. H., Chen, F., Miao, S., Tewari, M., Voogt, J. A., & Myint, S. (2015). Enhancing hydrologic modelling in the coupled Weather Research and Forecasting–urban modelling system. *Boundary-Layer Meteorology*, *155*(1), 87-109. https://doi.org/10.1007/s10546-014-9991-6

Yang, J., Hu, L., & Wang, C. (2019). Population dynamics modify urban residents' exposure to extreme temperatures across the United States. *Science Advances*, *5*(12), eaay3452. https://doi.org/10.1126/sciadv.aay3452

Yik, F. W. H., Burnett, J., & Prescott, I. (2001). A study on the energy performance of three schemes for widening application of water-cooled air-conditioning systems in Hong Kong. *Energy and Buildings*, *33*(2), 167–182. https://doi.org/10.1016/S0378-7788(00)00095-5

Yuan, C., Adelia, A. S., Mei, S., He, W., Li, X.-X., & Norford, L. (2020). Mitigating intensity of urban heat island by better understanding on urban morphology and anthropogenic heat dispersion. *Building and Environment*, *176*, 106876. https://doi.org/10.1016/j.buildenv.2020.106876

Zhang, N., Wang, X., Chen, Y., Dai, W., & Wang, X. (2016). Numerical simulations on influence of urban land cover expansion and anthropogenic heat release on urban meteorological environment in Pearl River Delta. *Theoretical and Applied Climatology*, *126*(3), 469–479. https://doi.org/10.1007/s00704-015-1601-0

Zheng, Y., Ren, C., Xu, Y., Wang, R., Ho, J., Lau, K., & Ng, E. (2018). GIS-based mapping of Local Climate Zone in the high-density city of Hong Kong. *Urban Climate*, *24*, 419–448. https://doi.org/10.1016/j.uclim.2017.05.008

Zhou, Y., Guan, H., Huang, C., Fan, L., Gharib, S., Batelaan, O., & Simmons, C. (2019). Sea breeze cooling capacity and its influencing factors in a coastal city. *Building and Environment*, *166*, 106408. https://doi.org/10.1016/j.buildenv.2019.106408

Zhu, R., Wong, M. S., Guilbert, É., & Chan, P.-W. (2017). Understanding heat patterns produced by vehicular flows in urban areas. *Scientific Reports*, *7*(1), 16309. https://doi.org/10.1038/s41598-017-15869-6